ANALYSES OF FATIGUE AND FATIGUE-CRACK GROWTH UNDER CONSTANT- AND VARIABLE-AMPLITUDE LOADING

J. C. Newman, Jr.
Mechanics of Materials Branch
NASA Langley Research Center
Hampton, Virginia USA 23681

ABSTRACT

Studies on the growth of small cracks have led to the observation that fatigue life of many engineering materials is primarily "crack growth" from micro-structural features, such as inclusion particles, voids, slip-bands or from manufacturing defects. This paper reviews the capabilities of a plasticity-induced crack-closure model to predict fatigue lives of metallic materials using "small-crack theory" under various loading conditions. Constraint factors, to account for three-dimensional effects, were selected to correlate large-crack growth rate data as a function of the effective stress-intensity factor range (ΔK_{eff}) under constant-amplitude loading. Modifications to the ΔK_{eff}-rate relations in the near-threshold regime were needed to fit measured small-crack growth rate behavior. The model was then used to calculate small- and large-crack growth rates, and to predict total fatigue lives, for notched and un-notched specimens under constant-amplitude and spectrum loading. Fatigue lives were predicted using crack-growth relations and micro-structural features like those that initiated cracks in the fatigue specimens for most of the materials analyzed. Results from the tests and analyses agreed well.

INTRODUCTION

The observation that small or short fatigue cracks can: (1) grow more rapid than those predicted by linear-elastic fracture mechanics (LEFM) based on large-crack data, and (2) grow at ΔK levels well below the large-crack threshold, has attracted considerable attention in the last two decades [1-5]. Some consensus is emerging on crack dimensions, mechanisms, and possible methods to correlate and to predict small-crack behavior. A useful classification of small cracks has been made by Ritchie and Lankford [6]. Naturally-occurring (three-dimensional) small cracks, often approaching microstructural dimensions, are largely affected by crack shape (surface or corner cracks), enhanced crack-tip plastic strains due to micro-plasticity, local arrest at grain boundaries, and the lack of crack closure in the early stages of growth. Whereas, two-dimensional short cracks, about 100 μm or greater, are through-thickness cracks which have been created artificially be removing the wake of material from large through cracks. Their behavior appears to be controlled by the plastic-wake history left by the large-crack growth process and the crack-growth rates are averaged over many grains through the thickness.

Over the last two decades, in the treatment of microstructurally-, mechanically-, and physically-small cracks, two basic approaches have emerged to explain the rapid growth and deceleration of small cracks when compared to large-crack growth behavior. The first is

characterized by “grain-boundary” blocking and consideration of microstructural effects on small-crack growth rates (see refs. 7 and 8). The second is a “continuum mechanics” approach accounting for the effects of material nonlinearity on the crack-tip driving force and crack-closure transients (see refs. 9 and 10).

The microstructural barrier model, developed by Miller and co-workers [5,8], was conceived to separate regimes of “microstructurally-small” cracks and “physically-small” cracks. The regime of microstructurally-small cracks (MSC) occurs when crack lengths are less than a dominant microstructural barrier, such as the grain size. Various researchers consider this regime to be synonymous with growth of a crack across a single grain or several grain diameters. For example, a crack may initiate at an inclusion particle on a grain boundary, propagate, slow down, and stop at the next grain boundary. With further cycling, or if the stress level is increased, this barrier can be overcome and the crack will propagate to the next barrier. Several different microstructural barriers to crack growth may exist in a single material because of material anisotropy and texture. The physically-small crack (PSC) regime is defined for crack lengths greater than the spacing of these dominant barriers. Miller [8] suggests that the complexities near micro-structural barriers in the MSC and PSC regimes hinder theoretical analyses of small-crack growth behavior based on LEFM parameters and he emphasizes the development of empirical equations, based on extensive test data, to determine constants in these relations. However, progress has been made in the analyses of cracks growing from inclusions (see ref. 11) and interacting with grain boundaries [12,13]. These analyses may be useful in developing the LEFM relations for cracks growing in complex microstructures.

Small-crack initiation and growth is a three-dimensional process with cracks in the depth, a, and length, c, directions interacting with the grain boundaries at different times in their cyclic history. Whereas, an observed crack in the length direction may have decelerated at or near a grain boundary, the crack depth may still be growing. As the crack grows in the depth direction, the rise in the crack-driving force at the c-location contributes to the crack penetrating that barrier. As the cracks become longer, the influence of grain boundaries become less as the crack front begins to average behavior over more grains. Small-crack growth deceleration may or may not occur depending upon the orientation of the adjacent grains [7]. A probabilistic analysis would be required to assess the influence of the variability of the grain structure on crack-growth rate properties. From an engineering standpoint, however, a weak-link or worst case scenario of grain orientation may provide a conservative estimate for the growth of small cracks through a complex microstructure. This is the basis for the continuum mechanics approaches.

It has been argued that the calculation of ΔK for a small crack growing from an inclusion could be in error (Schijve [14]). For example, if crack initiation occurs at a subsurface inclusion with subsequent breakthrough to the surface, a considerable elevation in ΔK is possible over that calculated from surface observations. Although the use of ΔK to characterize the growth of small cracks has proved to be convenient, its universal application has been viewed with some skepticism. Despite the above qualifications, research work on the growth of naturally-initiated small cracks, notably by Lankford [7,15] and the AGARD studies [16,17], have demonstrated the usefulness of the ΔK concept.

One of the leading continuum mechanics approaches to small-crack growth is that of Newman et al. [10,18]. The crack-closure transient (or more correctly the lack of closure in the early stages of growth) has long been suspected as a leading reason for the small-crack effect. The Newman crack-closure model [19] has demonstrated the capability to model small-crack growth behavior in a wide variety of materials and loading conditions [10,16-18]. Difficulties still exist for large-scale plastic deformations at holes or notches but these problems can be treated with advanced continuum mechanics concepts.

The purpose of this paper is to review the capabilities of the plasticity-induced crack-closure model [19] to correlate large-crack growth rate behavior and to predict fatigue lives in three aluminum alloys, a titanium alloy and a steel under various load histories using small-crack theory. Test results from the literature on 2024-T3, 7075-T6 and LC9cs aluminum alloys, Ti-6Al-4V titanium alloy and 4340 steel under constant-amplitude loading were analyzed with the closure model to establish an effective stress-intensity factor range (ΔK_{eff}) against crack-growth rate relation. The ΔK_{eff}-rate relation and the inclusion particle (or void) sizes that initiated cracks in these materials (except for the titanium alloy) were used in the model to predict total fatigue lives on notched specimens under various load histories. An equivalent-initial-flaw size (EIFS) concept was used for the titanium alloy. The load histories considered were constant-amplitude loading at various stress ratios ($R = S_{min}/S_{max}$) and two aircraft load spectra, Mini-TWIST (Lowak et al. [20]) and Felix-28 (Edwards and Darts [21]). Crack configurations used in these analyses were middle-crack tension, M(T), or compact tension, C(T), specimens for large-crack growth rate data, and three-dimensional crack configurations, such as a surface crack in a plate, a surface- or corner-crack at a hole or semi-circular edge notch for small-crack behavior. Comparisons are made between measured and predicted fatigue lives on various notched specimens.

CRACK AND NOTCH CONFIGURATIONS ANALYZED

The large-crack DK-rate data for the aluminum alloys [17,22] and steel [23] were obtained from M(T) specimens, whereas the data for the titanium alloy was obtained from C(T) specimens (see ref. 24). The fatigue specimens analyzed are shown in Figure 1. They were: (a) uniform stress ($K_T = 1$) un-notched specimen, (b) circular-hole ($K_T = 3.23$) specimen, (c) single-edge-notch tension, SENT, ($K_T = 3.15$ or 3.3) specimen, and (d) double-edge-notch tension ($K_T = 3.1$). All specimens were chemically polished to remove a small layer of disturbed material which may have contained some machining residual stresses. Here the stress concentration factor, K_T, is expressed in terms of remote (gross) stress, S, instead of the net-section stress.

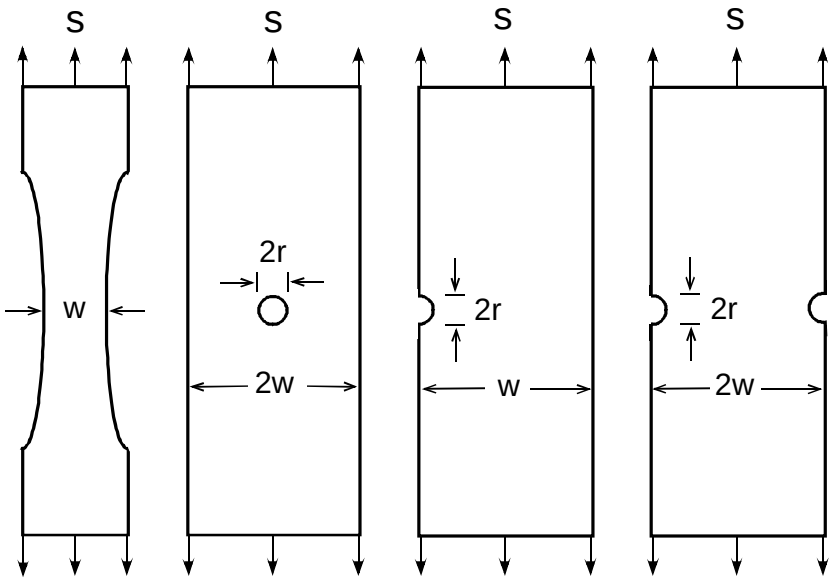

(a) $K_T = 1$ (b) $K_T = 3.23$ (c) $K_T = 3.15$ or 3.3 (d) $K_T = 3.1$

Figure 1. Specimens analyzed with "small-crack theory".

LARGE-CRACK GROWTH RATE BEHAVIOR

To make life predictions, ΔK_{eff} as a function of the crack-growth rate must be obtained for the material of interest. Fatigue crack-growth rate data should be obtained over the widest possible range in rates (from threshold to fracture), especially if spectrum load predictions are required. Data obtained on the crack configuration of interest would be helpful but it is not essential. Most damage-tolerant life calculations can be performed using linear elastic stress-intensity factor analysis with crack-closure modifications. In the following, the ΔK_{eff}-rate relation will be developed for only one of the aluminum alloys. Similar procedures were used to establish the relationships for all materials used in this study.

The linear-elastic effective stress-intensity factor range developed by Elber [25] is

$$\Delta K_{eff} = (S_{max} - S_o) \sqrt{(\pi c)} \; F(c/w) \tag{1}$$

where S_{max} is the maximum stress, S_o is the crack-opening stress, and F is the boundary-correction factor. However, for high stress-intensity factors, proof testing, and low-cycle fatigue conditions, the linear-elastic analyses are inadequate and nonlinear crack-growth parameters are needed. To account for plasticity, a portion of the Dugdale cyclic-plastic-zone length (ω) has been added to the crack length, c. The cyclic-plastic-zone-corrected effective stress-intensity factor [26] is

$$(\Delta K_p)_{eff} = (S_{max} - S_o) \sqrt{(\pi d)} \; F(d/w) \tag{2}$$

where $d = c + \omega/4$ and F is the cyclic-plastic-zone corrected boundary-correction factor. The cyclic plastic zone is given by

$$\omega = (1 - R_{eff})^2 \, \rho/4 \tag{3}$$

where $R_{eff} = S_o/S_{max}$ and the plastic-zone size (ρ) for a crack in a large plate is

$$\rho = c \{\sec[\pi S_{max}/(2\alpha\sigma_o)] - 1\} \quad (4)$$

where α is a constraint factor [19] and σ_o is the flow stress. Herein, the cyclic-plastic-zone corrected effective stress-intensity factor range will be used in the fatigue-life predictions.

The ΔK-rate data for large cracks in the 7075-T6 alloy are shown in Figure 2. These data were generated at two different laboratories [27] using M(T) specimens for three stress ratios (R). The data at each stress ratio parallel each other quite well. The data at each stress ratio show several knees or transitions, which are sharp changes in slope and these transitions occur at nearly the same crack-growth rate. Reference 27 discusses the relevance of some of these transtions.

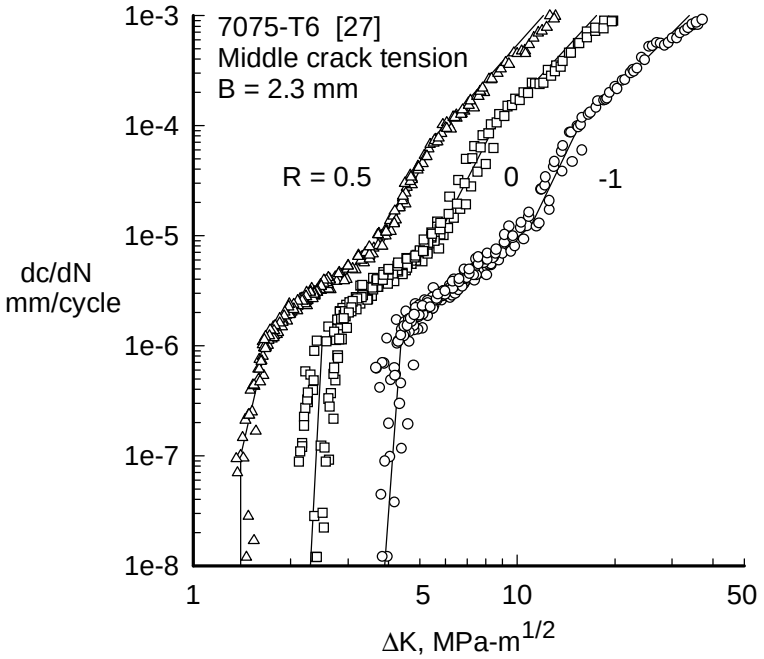

Figure 2. Stress-intensity factor range against rate for large cracks in 7075-T6 alloy.

The ΔK-rate data, shown in Figure 2, and additional data at high rates from reference 28, were used to establish the ΔK_{eff}-rate relation by using a crack-closure analysis. The only unknown in the closure analysis is the constraint factor, α. The constraint factor is determined by finding (by trial-and-error) a value that will correlate the crack-growth rate data over a wide range in stress ratios, as shown by Newman [29]. This correlation should produce a unique relationship between ΔK_{eff} and rate. In the large-crack threshold regime, the plasticity-induced closure model may not be able to collapse the threshold (ΔK-rate) data onto a unique ΔK_{eff}-rate relation because of other forms of closure. Roughness- and oxide-induced closure appear to be more relevant in the threshold regime than plasticity-induced closure. This may help explain why the constraint factors needed to correlate crack-growth rate data in the low-rate regime are lower than plane-strain conditions ($\alpha = 3$). The constraint factors are 1.7 to 2 for aluminum alloys, 1.9 to 2.2 for titanium alloys and 2.5 for steel. Several references

[10,16,18 and 27] have shown that large-crack threshold data (determined from the load-reduction procedures) are not applicable for small cracks. However, further study is needed to assess the interactions between plasticity-, roughness- and oxide-induced closure in this regime. If the plasticity-induced closure model is not able to give a unique ΔK_{eff}-rate relation in the threshold regime, then high stress ratio ($R \geq 0.7$) data may be used to help establish the ΔK_{eff}-rate relation in this regime. Small-crack test data and fatigue endurance limit data were used to help determine the small-crack effective threshold, $(\Delta K_{eff})_{th}$, values used herein.

The large-crack ΔK_{eff}-rate results for aluminum alloy 7075-T6 is shown in Figure 3. The data collapsed into a narrow band with several transitions in slope occurring at about the same rate for all stress ratios. Some differences were observed in the near threshold regime. For these calculations, a constraint factor (α) of 1.8 was used for rates less than 7E-04 mm/cycle and α equal to 1.2 was used for rates greater than 7E-03 mm/cycle. For intermediate rates, α was varied linearly with the logarithm of rate (see ref. 30). The values of α and rate were selected by trial-and-error and from analyses of crack growth under spectrum loading (see ref. 31). The constraint-loss regime (α = 1.8 to 1.2) has also been associated with the flat-to-slant crack-growth behavior. Reference 31 has developed an expression to predict the location of the flat-to-slant crack-growth regime and the effective stress-intensity factor at this transition is given by

$$(\Delta K_{eff})_T = 0.5\ \sigma_o\ \sqrt{B} \qquad (5)$$

For the 7075-T6 alloy sheet, $(\Delta K_{eff})_T$ = 13.1 MPa$\sqrt{m}$ (dashed line in Fig. 3). The width of the constraint-loss regime, in terms of rate or ΔK_{eff}, is a function of thickness, but this

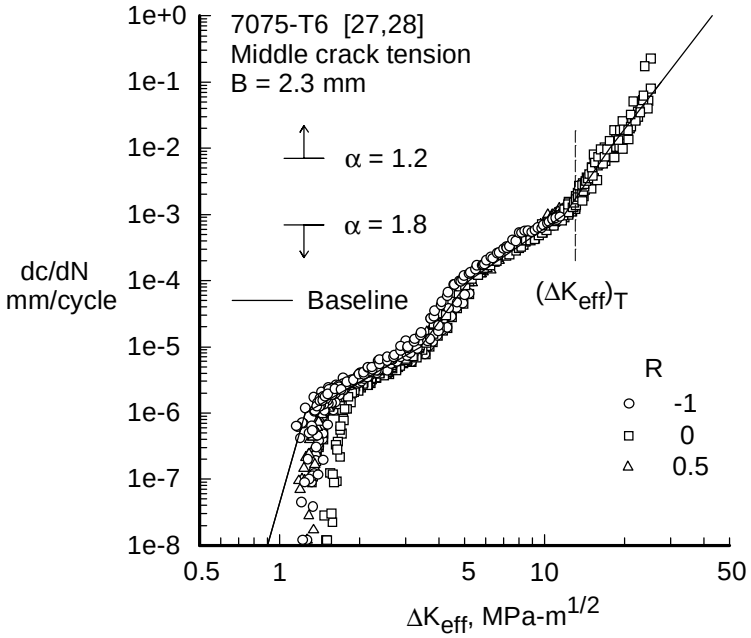

Figure 3. Effective stress-intensity factor range against rate for large cracks in 7075-T6 alloy.

relationship has yet to be developed. In the low crack-growth rate regime, near and at threshold, tests and analyses [10] have indicated that the threshold develops because of a rise

in the crack-opening stress due to the load-shedding procedure. In the threshold regime then, the actual ΔK_{eff}-rate data would lie at lower values of ΔK_{eff} because the rise in crack-opening stress was not accounted for in the current analysis. For the present study, an estimate was made for this behavior on the basis of small-crack data [27] and the results are shown by the solid line below rates of about 1E-06 mm/cycle. The baseline relation shown by the solid lines will be used later to predict fatigue lives under constant-amplitude and spectrum loading.

SMALL-CRACK GROWTH RATE BEHAVIOR

In the following sections, comparisons are made between small- and large-crack results on three aluminum alloys and a steel under laboratory air and room temperature conditions. The baseline effective stress-intensity factor range against crack-growth rate curve for each material was obtained from reference [32] and was used to predict small-crack growth rate behavior from extremely small initial crack sizes on the specimens shown in Figure 1.

Aluminum Alloy 7075-T6

Earlier work by Pearson [1] on fatigue-crack initiation and growth of small cracks from inclusion particles in two aluminum alloys (BS L65 and DTD 5050) set the stage for the development of small-crack theory. His results are shown in Figure 4, as the dotted curve, along with additional small-crack data (light solid curves) from Lankford [7] on 7075-T6 aluminum alloy using un-notched ($K_T = 1$) specimens. Lankford's data went down to ΔK values as low as 1.5 MPa$\sqrt{m}$. They both concluded that cracks of about the average grain size grew several times faster than large cracks at nominally identical ΔK values. The open symbols and dash-dot curve show the large-crack data and the development of the large-crack threshold at about 3 to 4 MPa$\sqrt{m}$. Some general observations from Lankford were that the minimum in dc/dN occurred when the crack length, c, was about the minimum dimension of the grain size and that the magnitude of the lower rates was controlled by the degree of micro-plasticity in the next grain penetrated by the crack. If the next grain is oriented like the first, then no deceleration will occur, as indicated by the uppermost small-crack curves.

At this stage, it would be of interest to compare the test results from Pearson and Lankford with the small-crack growth predictions made from the continuum-mechanics model based on crack closure [10,18]. The baseline ΔK_{eff}-rate relation used in the closure model is shown by dashed lines in Figure 4 [32]. The constraint factor (α) used in the FASTRAN code [30] was 1.8 for rates less than 7E-4 mm/cycle [32]. The ΔK_{eff}-rate results were generated from large-crack data for rates greater than about 2E-6 mm/cycle. The lower section of the ΔK_{eff}-rate relation (below 2E-6 mm/cycle) was estimated on the basis of small-crack data [27].

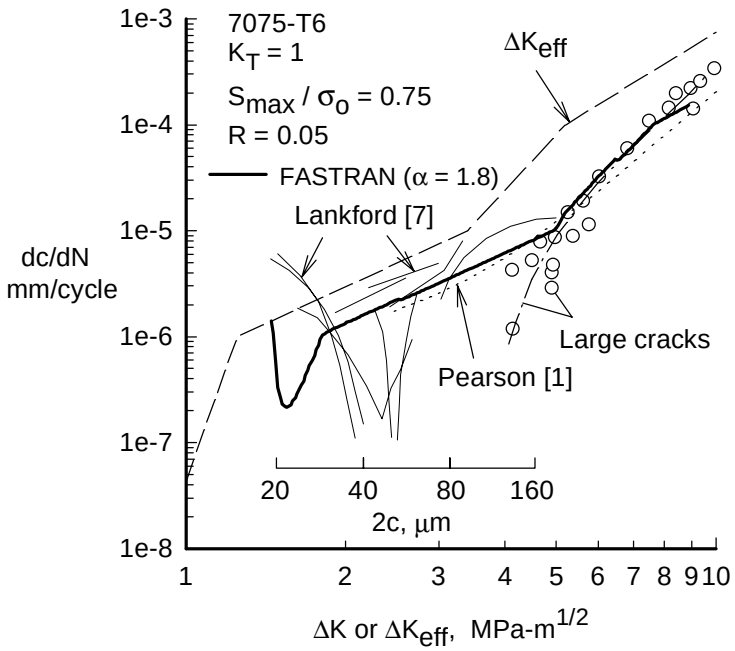

Figure 4. Measured and predicted small surface-crack growth in 7075-T6.

Because small cracks are assumed to be fully open on the first cycle, the ΔK_{eff}-rate relation is the starting point for small-crack analysis. The results of an analysis of the test specimen used by Lankford is shown by the heavy solid curve. The initial defect was selected as a 10-μm radius semi-circular surface crack. As the small crack grew, the closure level increased much faster than the ΔK level and a rapid decrease in rates was calculated. The rapid drop is a combination of the closure transient and the sharp change in slope of the ΔK_{eff}-rate relation (at about 1E-6 mm/cycle). At about 30 μm, the crack-opening stresses had nearly stabilized. The predicted small-crack results are in excellent agreement with Pearson's data and agree with some of Lankford's data which did not exhibit a grain-boundary influence. But interestingly, the small-crack analysis showed a single dip in the small-crack curve, similar to the "single" dip observed in some of Lankford's small-crack data. Would the grain-boundary interaction always occur at the same crack length (40 μm)? Why aren't there other dips, or small indications of a dip, in the rate curve at 80 or 120 μm? Similarly, a shift in the ΔK_{eff}-rate relation to higher ΔK_{eff} values in the near-threshold regime and considering a larger initial defect would also shift the analysis "dip" to higher ΔK values, closer to the test data. Further study is needed to help resolve these issues.

Small-crack data [27] have been generated on SENT specimens (Fig. 1c) made of 7075-T6 bare aluminum alloy (B = sheet thickness = 2.3 mm); and some of these data at R = -1 are shown in Figure 5. Specimens had a notch radius of 3.18 mm and a width (w) of 50 mm. The small-crack data was obtained by using the plastic-replica method. Scanning-electron microscope (SEM) photograph of a replica of a small crack at the notch surface is shown in Figure 6(a). In the calculation of ΔK for small surface cracks at the notch root, the crack-half-depth-to-crack-length (a/c) ratio was 1.0. (Note that for a surface crack at a notch root, the crack

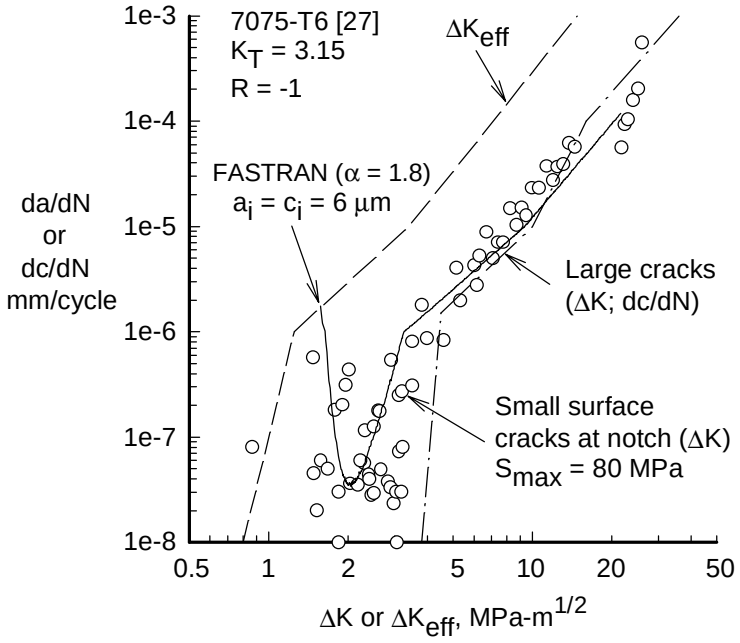

Figure 5. Measured and predicted small surface crack growth at a notch in 7075-T6.

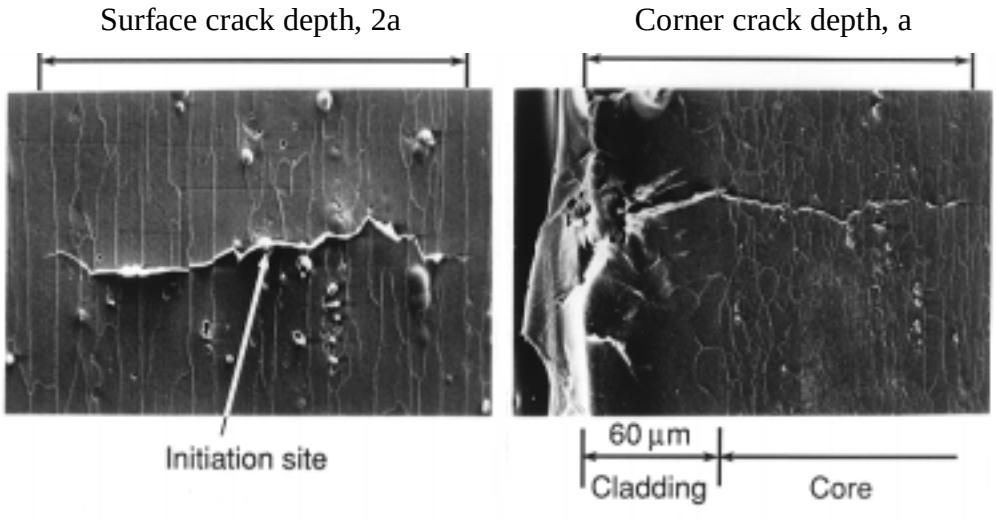

(a) Surface crack in 7075-T6 alloy (b) Corner crack in LC9cs clad alloy.

Figure 6. SEM photographs of replicas of notch-root surfaces with small crack (after [27]).

depth, 2a, is measured in the sheet thickness, B, direction.) The dashed curve is the ΔK_{eff}-rate (da/dN) relation; and the dashed-dot curve shows the ΔK-rate (dc/dN) relation for large cracks. Although the test data showed a large amount of scatter, the analysis (solid curve) agreed reasonably well with the trends in the test data. The initial 6-mm semi-circular surface defect is very close to the inclusion particle (or void) sizes that initiated cracks at the notch root [27]. In the low-rate regime, near the large-crack threshold, the predictions did not agree as well with the test data, probably because the replica method had an affect on crack-growth rates [27]. Fatigue tests

conducted with the plastic-replica method gave fatigue lives a factor of 3 to 4 times longer than those without the replica method. It was found that acetone, used in the replica method, protected the crack front from moisture in the laboratory air.

Aluminum Alloy LC9cs

The LC9cs alloy is equivalent to the 7075-T6 alloy except that the material had a cladding layer, as shown in Figure 6(b). Whereas surface cracks initiated at inclusion particles along the notch root in the 7075-T6 alloy, corner cracks were quite dominate in the clad alloy due to the cladding layer [27]. Figure 7 shows comparisons of measured and predicted rates on the LC9cs alloy for R = -1 loading (B = 2 mm) at S_{max} = 70 and 90 MPa. The solid curves show the predicted results with a 77-μm initial corner crack for several values of S_{max}. The initial defect was the clad-layer thickness plus inclusion particle (or void) sizes in the core (bare) material. A detailed description of the stress-intensity factor analysis of a corner crack emanating from a clad layer is given in reference 27. Again, all predictions start on the DK_{eff}-rate curve because the initial crack is assumed to be fully open on the first cycle. As the corner crack grew, the residual-plastic deformations built along the crack surfaces and caused the crack-opening stresses to stabilize at the large-crack conditions. Here, the predictions began to agree with the large-crack results. The predictions from the model agree well with the test data for S_{max} = 70 to 90 MPa in the early stages of crack growth, but the predicted rates were slightly low in the mid- to high-rate range. At S_{max} = 50 MPa, the predictions show a large drop in crack-growth rates, similar to that for the 7075-T6 alloy. This drop in rate is caused by the crack-closure transient and the shape of the ΔK_{eff}-rate curve. The crack would have been predicted to arrest if S_{max} was 40 MPa using $(\Delta K_{eff})_{th}$ = 0.9 MPa√m. The fatigue limit for notch specimens at R = -1 was about 40 MPa [27].

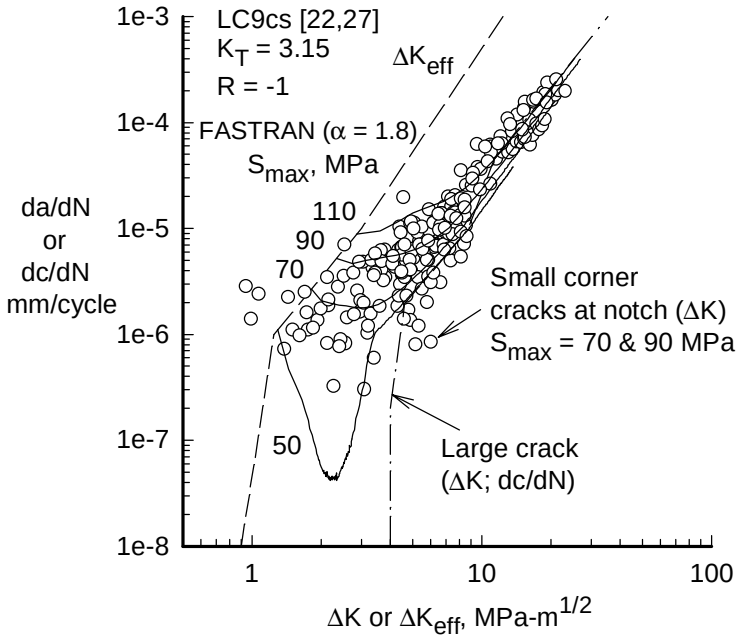

Figure 7. Measured and predicted small corner crack growth at a notch in LC9cs.

Whereas the small surface-crack data on the 7075-T6 bare alloy was affected by the plastic-replica method, the small corner-crack data on the LC9cs clad alloy did not appear to be affected. The clad alloy initiated predominately corner cracks and the replica was only applied along the notch root, thus it was surmised that the moisture from the laboratory air could reach the crack front by way of the crack on the specimen surface. Fatigue tests conducted on specimens with or without the plastic-replica method [27] produced nearly identical fatigue lives.

Aluminum Alloy 2024-T3

Figure 8 shows a comparison of small-crack data on SENT specimens [17] and large-crack data on M(T) specimens [33] made of the 2024-T3 alloy. The small-crack data, shown by the symbols, is only a small part of the overall database on this alloy. These results at R = 0 were taken from one laboratory and at an applied stress level of 110 MPa. This alloy showed a very large difference between the large-crack threshold (about 3 MPa$\sqrt{m}$) and small-crack growth behavior. Small cracks grew at ΔK values as low as 0.75 MPa$\sqrt{m}$. But for ΔK values greater than 3 MPa$\sqrt{m}$, the small- and large-crack data agreed quite well. The solid curve is the predicted rates from the FASTRAN closure model using the baseline ΔK_{eff}-rate curve (dashed lines). The initial defect was selected as a 6-μm radius surface crack located at the center of the notch. For the R = 0 condition, the small-crack effect (initial drop in rates at a ΔK value of about 1 MPa$\sqrt{m}$) is quite small. The crack-opening stresses from the model had stablized after a small amount of crack growth.

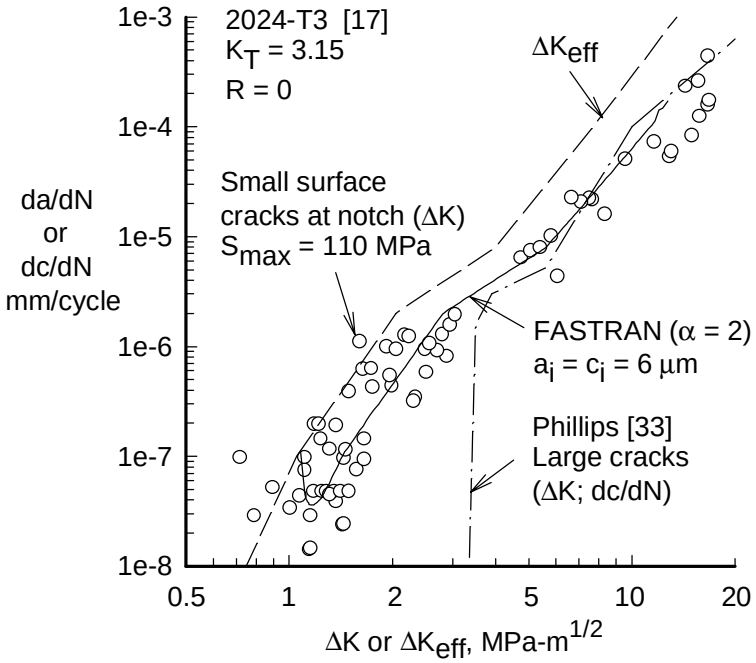

Figure 8. Measured and predicted small surface crack growth at a notch in 2024-T3.

High Strength 4340 Steel

Swain et al. [23] conducted small- and large-crack tests on 4340 steel. The large-crack results were obtained on middle-crack tension specimens tested at various stress ratios (R = -1, 0 and 0.5). The small-crack data were obtained from SENT specimens (Fig. 1c) with a notch radius of 3.2 mm and width w = 25.4 mm (K_T = 3.3) at the same stress ratios. Again, the plastic-replica method was used to measure the growth of small cracks. Examination of the initiation sites for 35 fatigue cracks gave information on the distribution of crack-initiation site dimensions. Two types of crack-initiation particles were observed: a spherical particle and a stringer particle. The spherical (calcium-aluminate) particle, shown in the SEM photograph in Figure 9, was by far the most dominate crack-initiation site particle.

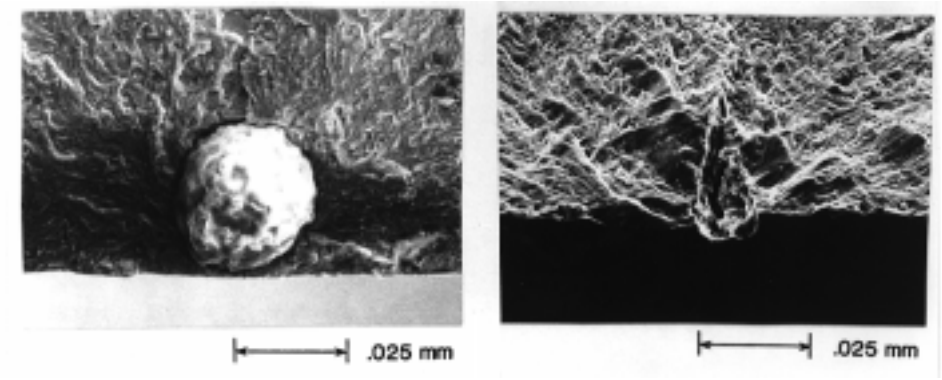

(a) (b)

Figure 9. Crack initiation site at (a) spherical-inclusion particle and (b) stringer particle in 4340 steel (after [23]).

The cumulative distribution function for these defects is plotted against an equivalent semi-circular defect radius based on the actual area of the defect in Figure 10. The mean defect was about 13-mm in radius. Selecting defects of 8- and 30-mm in radius covered over 80% of all defects.

A comparison of some of the small- and large-crack data on the 4340 steel is shown in Figure 11 at R = 0 conditions. The symbols show small surface-crack data from the SENT specimens. The dashed-dot curve is the large-crack data obtained from M(T) specimens. Note that the small cracks were measured in the a-direction and large cracks were measured in the c-direction. Here the small- and large-crack data agreed quite well. The small-crack effect appears to be less dominate at the positive stress-ratio conditions for a variety of materials [16,17]. Again, the dashed curve is the ΔK_{eff}-rate curve determined from the M(T) specimen data. The constraint factor (α) was 2.5 for rates less than 5E-4 mm/cycle [32]. The solid curves show the predicted results from the FASTRAN closure model with either an initial semi-circular surface crack of 8- or 30-μm with S_{max} = 360 MPa. Again, all predictions start on the ΔK_{eff}-rate curve because the initial crack is assumed to be fully open on the first cycle. Because the effective stress-intensity factor curve is near to the large-crack curve, small-crack effects are weak. The predicted results for the largest defect size rapidly approaches the large-crack behavior. But the predicted results for the smallest defect size showed a very rapidly drop and then a very rapid

rise to large-crack behavior. Again, this behavior is due to the crack-closure transient and the shape of the ΔK_{eff}-rate curve at low rates.

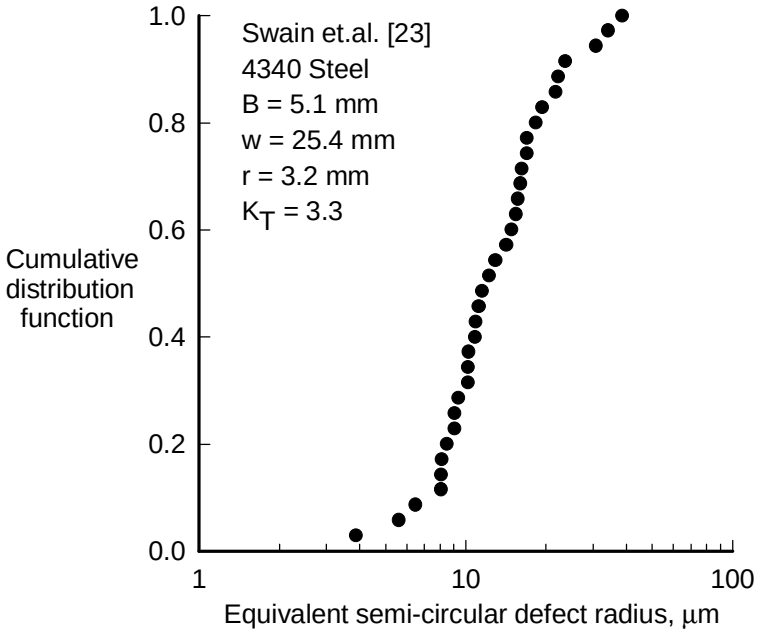

Figure 10. Cumulative distribution function for initiation sites in 4340 steel.

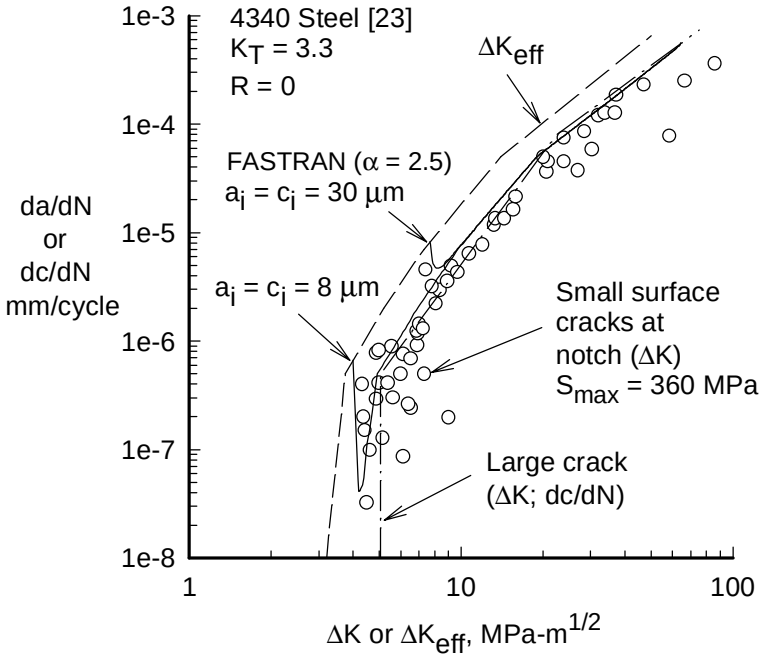

Figure 11. Measured and predicted small corner crack growth at a notch in 4340 steel.

PREDICTION OF FATIGUE LIFE USING SMALL-CRACK THEORY

Newman and co-workers [16-18,22,23,26,27] have used continuum-mechanics concepts with initial defect sizes, like those which initiated cracks at inclusion particles, voids or slip-bands, and the effective stress-intensity factor range against rate relations to predict the fatigue lives for many engineering materials. The baseline crack-growth rate data for these materials were obtained from large-crack data, in most cases ignoring the large-crack threshold, and using small-crack growth rates at extremely low rates. Small-crack thresholds were estimated from small-crack data and/or the endurance limits for these materials. In the following, some typical examples of using small-crack theory to predict fatigue behavior will be presented.

Aluminum Alloy 2024-T3

Grover et al. [34] conducted fatigue tests on flat (K_T = 1) dog-bone specimens (Fig. 1a) made of 2024-T3 aluminum alloy under R = 0 and -1 loading. The specimens were electro-polished but no information on crack-initiation sites was available. Thus, in the analyses it was assumed that cracks initiated as quarter-circular corner cracks. A comparison of experimental and calculated fatigue lives is shown in Figure 12. Various initial crack sizes were selected by trial-and-error to find the best value to fit the test data. Analyses with a 20-μm initial crack size fit the test data quite well for both R ratios. Results for each R ratio approached the flow stress σ_o (average of the yield stress and ultimate tensile strength) for high applied stress levels. Some discrepancies were observed for both R = 0 and -1 analyses at applied stress levels above the yield stress. These discrepancies were expected because the

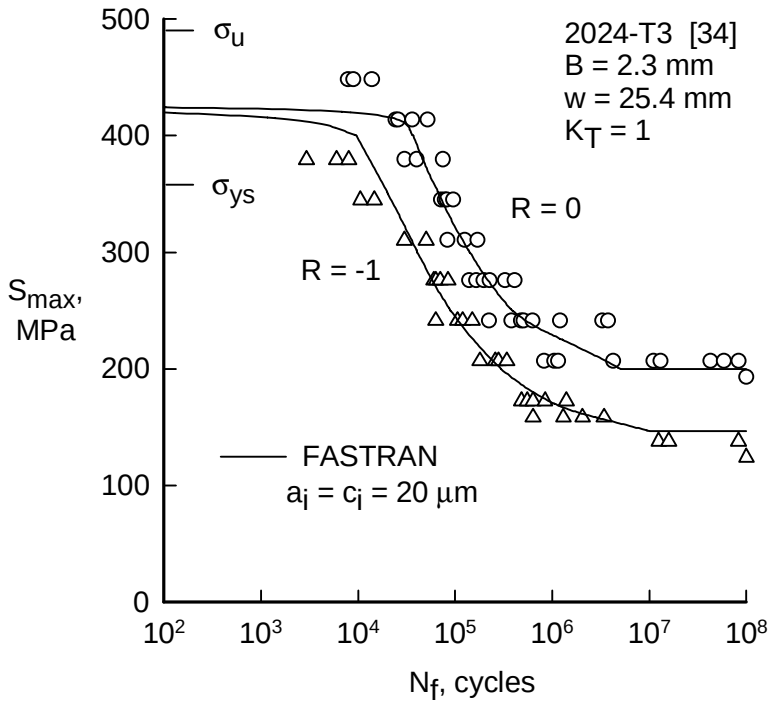

Figure 12. Measured and calculated fatigue lives for un-notched 2024-T3 specimens.

closure model does not account for strain-hardening effects but uses an average flow stress. To fit fatigue limits, a value of $(\Delta K_{eff})_{th}$ of 0.8 MPa$\sqrt{m}$ was needed for the 20-μm initial crack.

Aluminum Alloys LC9cs and 7075-T6

Fatigue tests were conducted on SENT specimens (Fig. 1c) made of the two aluminum alloys (LC9cs and 7075-T6) for various constant-amplitude stress ratios and under the Mini-TWIST [20] load spectrum. For each material, a single ΔK_{eff}-rate relation and the same initial defect size were used to make fatigue-life predictions assuming that the total fatigue life is composed on only crack propagation.

Constant-Amplitude Loading: The fatigue data for the LC9cs alloy under constant-amplitude loading (R = 0.5, 0 and -1) is shown in Figure 13 as symbols. A symbol with an arrow indicates that the test was terminated before failure. In the analysis, the initial crack size was $a_i = c_i$ = 77 μm (clad layer plus an inclusion particle size). This initial crack size is somewhat larger than the cladding-layer thickness, but it is consistent with observations made early in life [27]. The effective stress-intensity factor range against rate relation is given in reference 32 and the small-crack effective threshold, $(\Delta K_{eff})_{th}$, was assumed to be 0.9 MPa$\sqrt{m}$. The FASTRAN code [30] was then used to make life predictions. The solid curves show the predicted number of cycles to failure for the various stress ratios. Predictions agreed reasonable well with the test data. Similar comparisons on the 7075-T6 alloy are given in reference 27.

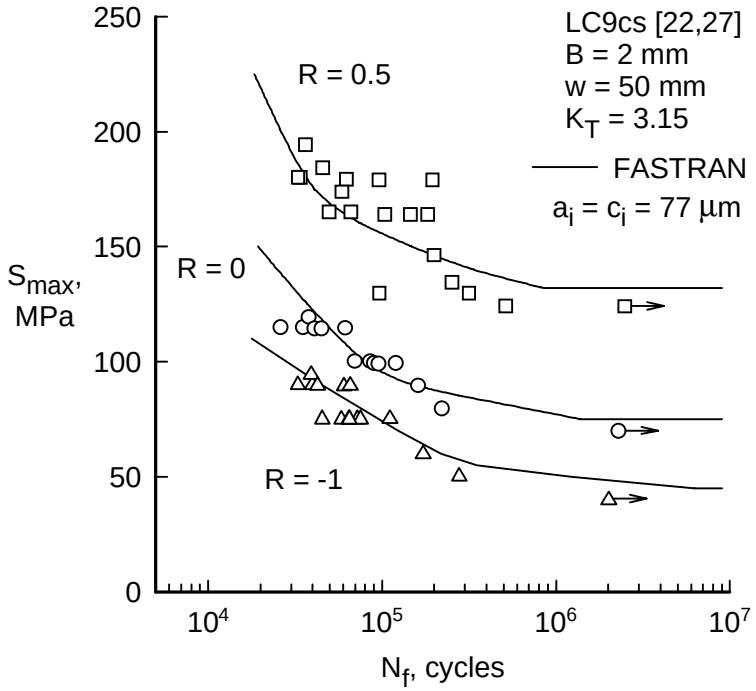

Figure 13. Measured and predicted fatigue lives for LC9cs aluminum alloy.

Mini-TWIST Spectrum Loading: Fatigue tests conducted on SENT specimens made of both LC9cs and 7075-T6 aluminum alloys are shown in Figure 14. The maximum stress level (S_{max}) in

the Mini-TWIST spectrum is plotted against the number of cycles to failure. For the same applied stress level, the clad alloy produced a shorter fatigue life than the bare alloy. Using the same crack-growth properties and initial defect sizes, as those used under constant-amplitude loading, FASTRAN was used to make fatigue-life predictions. Again, the predicted fatigue lives were in reasonable agreement with the test data.

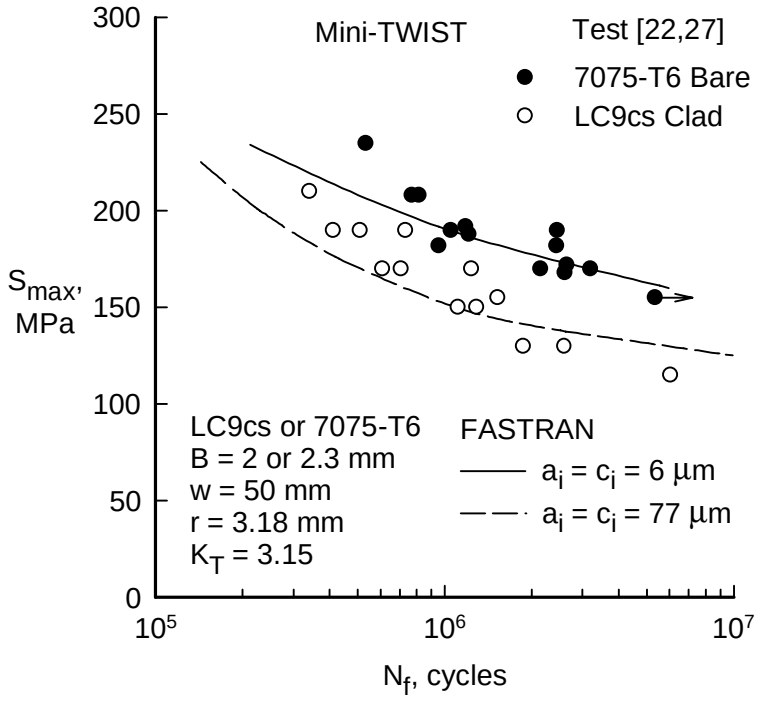

Figure 14. Measured and predicted fatigue lives for two aluminum alloys under Mini-TWIST.

In the fatigue analyses under the Mini-TWIST spectrum loading, the crack-closure model FASTRAN was used to calculate the crack-opening stress levels as a function of load history. The opening stresses were then used with the applied stresses to calculate the effective stress-intensity factor range and, subsequently, the crack-growth rate for each cycle. In the bare aluminum alloys, cracks have been found to initiate at inclusion-particle clusters or voids left when these particles were removed during machining or the polishing process. An initial material defect-void size (a_i, c_i, b) was selected for the crack growth simulations. The initial crack size was selected as a semi-circular defect ($a_i = c_i$ = 6 μm) located at the center of the notch and the defect-void half-height, b, was selected as 0.5 μm. The 0.5-μm value was selected so that the initial defect surface would not close even for R = -1 compressive loading (see ref. 27). Calculations are shown in Figure 15 for a Mini-TWIST spectrum with a mean flight stress S_{mf} = 73 MPa (S_{max} = 190 MPa). Here the crack-opening stress is plotted against the cyclic-life ratio (applied cycles N to N_f, cycles to failure). A variable-constraint option was selected for this simulation. Thus, α = 1.8 for rates less than 7.0E-4 mm/cycle and α = 1.2 for rates greater than 7.0E-3 mm/cycle. Only a small part of the opening stresses calculated from the model is shown in Figure 15. These results show that the opening stresses start near the minimum stress in the spectrum and rise as the crack grows. Crack-opening stresses generally leveled off at N/N_f = 0.6 to 0.9. The rapid jump in S_o at N/N_f about 0.92 is

caused by the change in constraint from 1.8 to 1.2 for the higher crack-growth rates. Incidentally, the surface crack became a through crack (2a = B) at N/N_f of about 0.9.

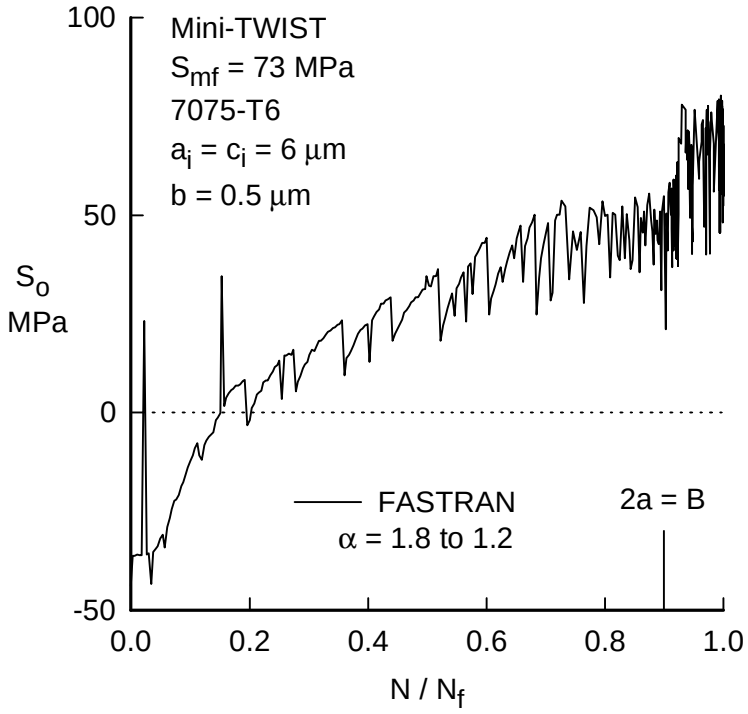

Figure 15. Calculated crack-opening stresses for small crack in 7075-T6 alloy under Mini-TWIST.

High-Strength 4340 Steel

Everett [35] conducted fatigue tests on 4340 steel (B = 3.2 mm) using a specimen with a single open hole (Fig. 1b) with a hole radius of 3.2 mm and a width w = 12.7 mm. Tests were conducted under both constant-amplitude and spectrum loading. The material used in this study had the same strength level as the material tested in reference 23, but the specimens were thinner and were taken from a different heat of material. However, it was assumed that the large-crack data and inclusion-particle sizes would be the same. A small-crack effective threshold, $(\Delta K_{eff})_{th}$, of 3.2 MPa$\sqrt{m}$ (see Fig. 11) was used to predict the endurance limits or the applied stress level where the initial defect would not grow.

Constant-Amplitude Loading: Figure 16 shows test data (symbols) obtained from open-hole specimens at a stress ratio R = 0. Using an 8- and 30-μm initial semi-circular surface crack located at the center of the hole, fatigue-life predictions were made. Near the endurance limit, the analyses bounded the test data quite well, but the analyses tended to predict slightly longer lives at the highest stress levels than the tests. The reason for this over prediction is not known. Surprisingly, the defect size had more influence on life in the endurance limit regime than at the higher stress levels.

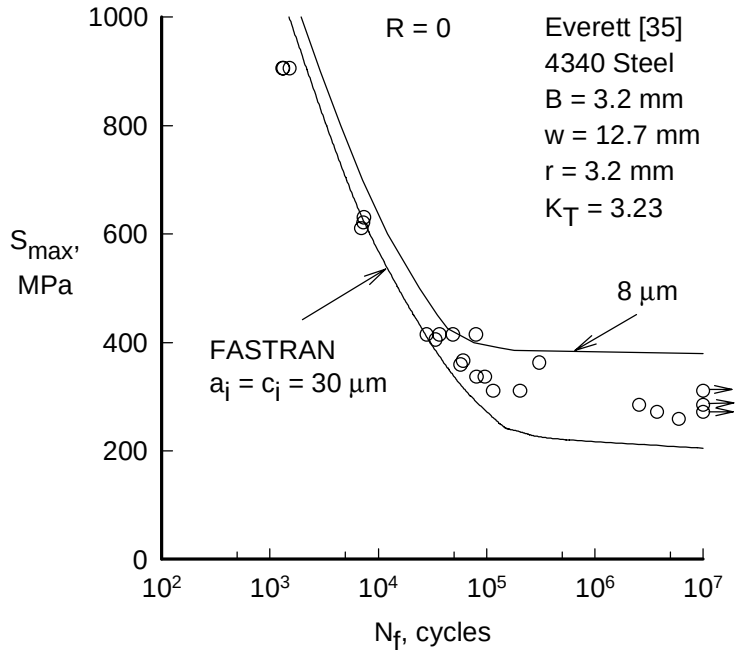

Figure 16. Measured and predicted fatigue lives for 4340 steel.

Felix-28 Spectrum Loading: Results of fatigue tests conducted under the Felix-28 load sequence are shown in Figure 17 as symbols. Again, the maximum stress in the spectrum is plotted against the cycles to failure. Predictions of total fatigue life under the Felix-28 load spectrum were made using the FASTRAN code [30] by calculating the number of cycles necessary to grow a crack from the assumed initial defect size, located at the center of the open hole, to failure. The predicted results for the two initial defect sizes bounded the test data quite well.

Titanium Alloy Ti-6Al-4V

A comparison of measured and calculated fatigue lives on two titanium forgings is shown in Figure 18. The fatigue test data was generated on double-edge-notch tensile specimens (Fig. 1d) made from the two forgings at R = 0.1 [36]. The notch radius was 2 mm and the width (2w) was 13.8 mm. The results from the two forgings agreed quite well with each other. Because no metallurgical examination of the fractured specimens was made to evaluate the initiation sites, an equivalent-initial-flaw size (EIFS) concept was used in the fatigue analyses. The FASTRAN life-prediction code [30] was used with large-crack growth rate data (determined from C(T) specimens, see ref. 24) and various size defects to calculate the fatigue lives. A flaw size of 2-mm (semi-circular surface crack located at the center of the notch) fit the upper bound of the test data and a 20-mm flaw fit the lower bound. The upper plateau is where the net-section stress is equal to 1.3 times the flow stress (σ_o = 920 MPa) of the material. In the model, the plastic zone extends across the net-section and the specimen fails when the net-section stress reaches the

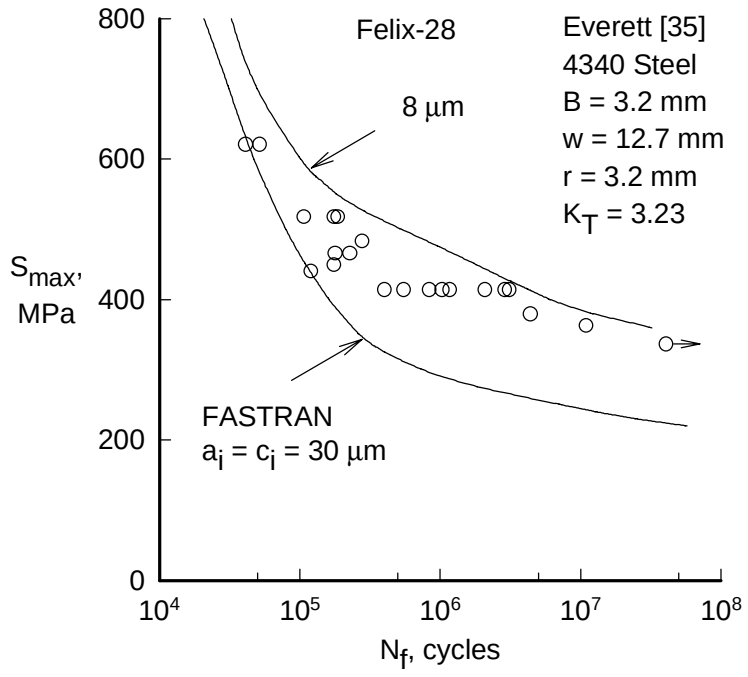

Figure 17. Measured and predicted fatigue lives for 4340 steel under Felix-28.

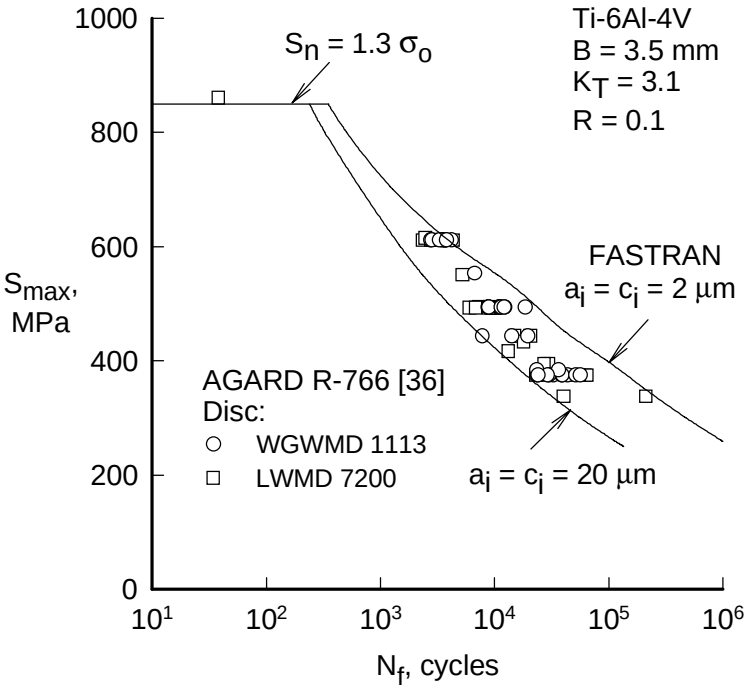

Figure 18. Measured and calculated fatigue lives for Ti-6Al-4V titanium alloy.

constraint factor (1.3) times the flow stress (see ref. 24). The single test data point tends to confirm the notch strengthen behavior of the specimen. However, in the analysis, the crack controls the

constraint factor (as shown in Fig. 3) but for notched specimens, the three-dimensional stress state around the notch also causes the flow stress to be elevated. Although the results shown in Figure 17 for the upper plateau are quite good, the agreement is fortuitous because notch strengthening has not been accounted for in the analysis. As mentioned earlier, difficulties still exist for large-scale plastic deformations at holes or notches. This area requires further study.

CONCLUDING REMARKS

A "plasticity-induced" crack-closure model was used to correlate large-crack growth rate data on three aluminum alloys, a titanium alloy, and a steel under constant-amplitude loading for a wide range of stress ratios. A constraint factor, which accounts for three-dimensional state-of-stress effects, was used in determining the effective stress-intensity factor range against rate relations. Comparisons made between measured and predicted small-crack growth rates showed that the closure model could predict the trends that were observed in the tests. Using the closure model and some microstructural features, such as inclusion-particle sizes or clad-layer thickness, a fatigue-life prediction method was demonstrated for most materials. An equivalent-initial-flaw size concept was used on the titaniumalloy. Predicted fatigue lives for notched specimens made of the aluminum alloys, titanium alloy and steel compared well with test data under constant-amplitude and spectrum loading.

For an engineering component, which may contain a large number of fastener holes and other areas of stress concentration, the likelihood of a critical size inclusion particle being located at one of these sites is large. Thus, using the largest material defect, such as the 30-μm defect for the steel or bare aluminum alloys, would produce a somewhat conservative but reliable life prediction from a materials standpoint. Ultimately, manufacturing defects, if larger than the material defects, would control the fatigue lives of components subjected to cyclic loading. The analyses presented herein should be able to predict the influence of these defects on life. To conclude, the test results and analyses presented herein did not have substantial residual stresses due to machining because all specimens were polished. But in practice, holes and machined parts may contain residual stresses. Accounting for these residual stresses is an important area to be studied in the future.

ACKNOWLEDGMENTS

The author takes this opportunity to thank his colleagues Mr. Ed Phillips and Dick Everett, Drs. Mary Swain, Peter Edwards and Xueren Wu. Their small- and large-crack test data, and their guidance, have contributed greatly to making Small-Crack Theory successful.

REFERENCES

[1] Pearson, S., "Initiation of Fatigue Cracks in Commercial Aluminum Alloys and the Subsequent Propagation of Very Short Cracks," Engineering Fracture Mechanics, Vol. 7, 1975, pp. 235-247.

[2] Kitagawa, H. and Takahashi, S., "Applicability of Fracture Mechanics to Very Small Cracks or the Behaviour in the Early Stages", Proceedings of Second International Conference on Mechanical Behavior of Materials, Boston, MA, 1976, pp. 627-631.
[3] Zocher, H., ed., "Behaviour of Short Cracks in Airframe Components", AGARD CP-328, 1983.
[4] Ritchie, R. O. and Lankford, J., eds., "Small Fatigue Cracks," The Metallurgical Society, Inc., Warrendale, PA, 1986.
[5] Miller, K. J. and de los Rios, E. R., eds., "The Behaviour of Short Fatigue Cracks," European Group on Fracture, Publication No. 1, 1986.
[6] Ritchie, R. O. and Lankford, J., "Overview of the Small Crack Problem", Small Fatigue Cracks, R. O. Ritchie and J. Lankford, eds., 1986, pp. 1-5.
[7] Lankford, J., "The Growth of Small Fatigue Cracks in 7075-T6 Aluminum," Fatigue of Engineering Materials and Structures, Vol. 5, 1982, pp. 233-248.
[8] Miller, K. J., "The Behaviour of Short Fatigue Cracks and their Initiation," Fatigue and Fracture of Engineering Materials and Structures, Vol. 10, 1987, pp. 93-113.
[9] El Haddad, M. H., Dowling, N. E., Topper, T. H. and Smith, K. N., "J Integral Application for Short Fatigue Cracks at Notches," International Journal of Fracture, Vol. 16, 1980, pp. 15-30.
[10] Newman, J. C., Jr., "A Nonlinear Fracture Mechanics Approach to the Growth of Small Cracks," Behaviour of Short Cracks in Airframe Components, Zocher, H., ed., AGARD CP-328, 1983, pp. 6.1-6.26.
[11] Trantina, G. G. and Barishpolsky, M., "Elastic-Plastic Analysis of Small Defects-Voids and Inclusions", Engineering Fracture Mechanics, Vol. 20, 1984, pp. 1-10.
[12] Nakai, Y., Tanaka, K. and Yamashita, M., "Analysis of Closure Behavior of Small Fatigue Cracks", Japan Society of Materials Science, Vol. 32, 1983, pp. 19-25.
[13] Tanaka, K., "Modeling of Propagation and Non-propagation of Small Fatigue Cracks," Small Fatigue Cracks, R. O. Ritchie and J. Lankford, eds., The Metallurgical Society, Inc., 1986, pp. 343-362.
[14] Schijve, J., "The Practical and Theoretical Significance of Small Cracks - An Evaluation," Fatigue 84, EMAS, Ltd., 1984, pp. 751-771.
[15] Lankford, J., "The Effects of Environment on the Growth of Small Fatigue Cracks," Fatigue of Engineering Materials and Structures, Vol. 6, 1983, pp. 15-32.
[16] Newman, J. C., Jr. and Edwards, P. R., "Short-Crack Growth Behaviour in an Aluminum Alloy - an AGARD Cooperative Test Programme," AGARD R-732, 1988.
[17] Edwards, P. R. and Newman, J. C., Jr., eds., "Short-Crack Growth Behaviour in Various Aircraft Materials," AGARD R-767, 1990.
[18] Newman, J. C., Jr., Swain, M. H. and Phillips, E. P., "An Assessment of the Small-Crack Effect for 2024-T3 Aluminum Alloy," Small Fatigue Cracks, The Metallurgical Society, Inc., Warrendale, PA, 1986, pp. 427-452.
[19] Newman, J. C., Jr., "A Crack Closure Model for Predicting Fatigue Crack Growth under Aircraft Spectrum Loading," Methods and Models for Predicting Fatigue Crack Growth under Random Loading, ASTM STP 748, 1981, pp. 53-84.
[20] Lowak, H., deJonge, J. B., Franz, J. and Schutz, D., "Mini-TWIST--A Shortened Version of TWIST", LBF Report No. TB-146, Laboratorium für Betriebsfestigkeit, Germany, 1979.

[21] Edwards, P. R. and Darts, J., "Standardised Fatigue Loading Sequences for Helicopter Rotors (Helix and Felix) - Part 2: Final Definition of Helix and Felix", RAE Technical Report 84085, 1984.
[22] Newman, J. C., Jr., Wu, X. R., Swain, M. H., Zhao, W., Phillips, E. P. and Deng, C. F., "Small-Crack Growth Behavior in High-Strength Aluminum Alloys - NASA/CAE Cooperative Program", 18th Congress of the International Council of Aeronautical Sciences, Beijing, China, 799-820 (1992).
[23] Swain, M. H., Everett, R. A., Newman, J. C., Jr. and Phillips, E. P., "The Growth of Short Cracks in 4340 steel and Aluminum-Lithium 2090," AGARD R-767, P. R. Edwards and J. C. Newman, Jr., eds., 1990, pp. 7.1-7.30.
[24] Newman, J. C., Jr., "Application of a Closure Model to Predict Crack Growth in Three Engine Disc Materials," International Journal of Fracture, Vol. 80, 1996, pp. 193-218.
[25] Elber, W., "The Significance of Fatigue Crack Closure," Damage Tolerance in Aircraft Structures, ASTM STP 486, 1971, pp. 230-242.
[26] Newman, J. C., Jr., "Fracture Mechanics Parameters for Small Fatigue Cracks," Small Crack Test Methods, ASTM STP 1149, J. Allison and J. Larsen, eds., 1992, pp. 6-28.
[27] Newman, J. C., Jr., Wu, X. R., Venneri, S. and Li, C., "Small-Crack Effects in High-Strength Aluminum Alloys," NASA RP-1309, 1994.
[28] Hudson, C. M., "Effect of Stress Ratio on Fatigue-Crack Growth in 7075-T6 and 2024-T3 Aluminum Alloy," NASA TN D-5390, 1969.
[29] Newman, J. C., Jr., "A Crack-Opening Stress Equation for Fatigue Crack Growth," International Journal of Fracture, Vol. 24, 1984, R131-R135.
[30] Newman, J. C., Jr., "FASTRAN-II - A Fatigue Crack Growth Structural Analysis Program," NASA TM 104159, 1992.
[31] Newman, J. C., Jr., "Effects of Constraint on Crack Growth under Aircraft Spectrum Loading," Fatigue of Aircraft Materials, A. Beukers et al., eds., Delft University Press, 1992, pp. 83-109.
[32] Newman, J. C., Jr., Phillips, E. P. and Swain, M. H., "Fatigue-Life Prediction Methodology using Small-Crack Theory," NASA TM 110307, 1997.
[33] Phillips, E. P., "The Influence of Crack Closure on Fatigue Crack Growth Thresholds in 2024-T3 Aluminum Alloy," ASTM STP 982, J. C. Newman, Jr. and W. Elber, eds., 1988, pp. 505-515.
[34] Grover, H. J., Hyler, W. S., Kuhn, P., Landers, C. B. and Howell, F. M., "Axial-Load Fatigue Properties of 24S-T and 75S-T Aluminum Alloy as Determined in Several Laboratories," NACA TN-2928, 1953.
[35] Everett, R. A., Jr., "A Comparison of Fatigue Life Prediction Methodologies for Rotorcraft", NASA TM 102759, 1990.
[36] Mom, A. J. A. and Raizenne, M. D., eds., "AGARD Engine Disc Cooperative Test Programme," AGARD Report 766, 1988.